JACS
JOURNAL OF THE AMERICAN CHEMICAL SOCIETY
pubs.acs.org/JACS
Article

Elucidation of the Roles of Water on the Reactivity of Surface Intermediates in Carboxylic Acid Ketonization on TiO_2

Fan Lin, Wenda Hu, Nicholas R. Jaegers, Feng Gao, Jian Zhi Hu,* Huamin Wang,* and Yong Wang*

Cite This: J. Am. Chem. Soc. 2023, 145, 99−109
Read Online
ACCESS | Metrics & More | Article Recommendations | Supporting Information

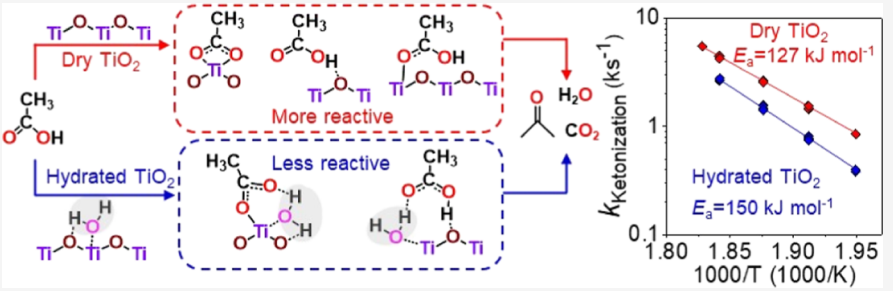

ABSTRACT: The effects of water on the carboxylic acid ketonization reaction over solid Lewis-acid catalysts were examined by nuclear magnetic resonance (NMR) spectroscopy, diffuse reflectance infrared Fourier transform spectroscopy (DRIFTS), temperature-programmed desorption (TPD), and kinetic measurements. Acetic acid and propanoic acid were used as model compounds, and P25 TiO_2 was used as a model catalyst to represent the anatase TiO_2 since the rutile phase only contributes to <2.5% of the overall ketonization activity of P25 TiO_2. The kinetic measurement showed that introducing H_2O vapor in gaseous feed decreases the ketonization reaction rate by increasing the intrinsic activation barrier of gas-phase acetic acid on anatase TiO_2. Quantitative TPD of acetic acid indicated that H_2O does not compete with acetic acid for Lewis sites. Instead, as indicated by combined approaches of NMR and DRIFTS, H_2O associates with the adsorbed acetate or acetic acid intermediates on the catalyst surface and alters their reactivities for the ketonization reaction. There are multiple species present on the anatase TiO_2 surface upon carboxylic acid adsorption, including molecular carboxylic acid, monodentate carboxylate, and chelating/bridging bidentate carboxylates. The presence of H_2O vapor increases the coverage of the less reactive bridging bidentate carboxylate associated with adsorbed H_2O, leading to lower ketonization activity on hydrated anatase TiO_2. Surface hydroxyl groups, which are consumed by interaction with carboxylic acid upon the formation of surface acetate species, do not impact the ketonization reaction.

1. INTRODUCTION

Carboxylic acids are important intermediates for converting biomass to fuels and chemicals. The major routes of biomass conversion, hydrolysis/fermentation, pyrolysis, and hydrothermal liquefaction, produce carboxylic acids. For example, bio-oils produced by biomass pyrolysis contain 10−50 wt % of carboxylic acids (e.g., acetic acid and propanoic acid);[1] the aqueous byproduct of biomass hydrothermal liquefaction contains short-chain carboxylic acids such as acetic acid and propionic acid,[2] whereas the sugars produced from biomass hydrolysis can be dehydrated and further hydrolyzed to levulinic and formic acids.[3] Ketonization of carboxylic acids forms ketones (eq 1), which are the building blocks that can undergo further aldol condensation to increase the fraction of molecules that fall in the gasoline/diesel molecular size range.[4−7]

$$R_1COOH + R_2COOH \rightarrow R_1COR_2 + CO_2 + H_2O \quad (R_1, R = \text{alkyl groups}) \quad (1)$$

Metal oxides (e.g., TiO_2, ZrO_2, ZnO, and CeO_2)[6,8−14] containing Lewis acid−base site pairs have been widely reported as efficient catalysts for carboxylic acid ketonization. There have been multiple ketonization mechanisms proposed on these metal oxides,[9] and the most widely accepted one is the β-ketoacid-based mechanism.[4,14−17] In this mechanism, the ketone product is formed upon the decarboxylation of a β-ketoacid intermediate, but different routes have been proposed for β-ketoacid formation, as depicted in Scheme 1. Both routes are initiated by the dissociation of carboxylic acid on the Lewis acid−base site pairs on the oxide surface forming carboxylate species (step 1). An enolate intermediate is formed upon α-H abstraction on a carboxylate (steps 2a and 2b). In one

Received: August 10, 2022
Published: December 23, 2022

https://doi.org/10.1021/jacs.2c08511
J. Am. Chem. Soc. 2023, 145, 99−109

Scheme 1. β-Ketoacid-Based Mechanism for Carboxylic Acid Ketonization on Metal Oxides (M = Metal Cation; R,R′ = H or Alkyl Groups)

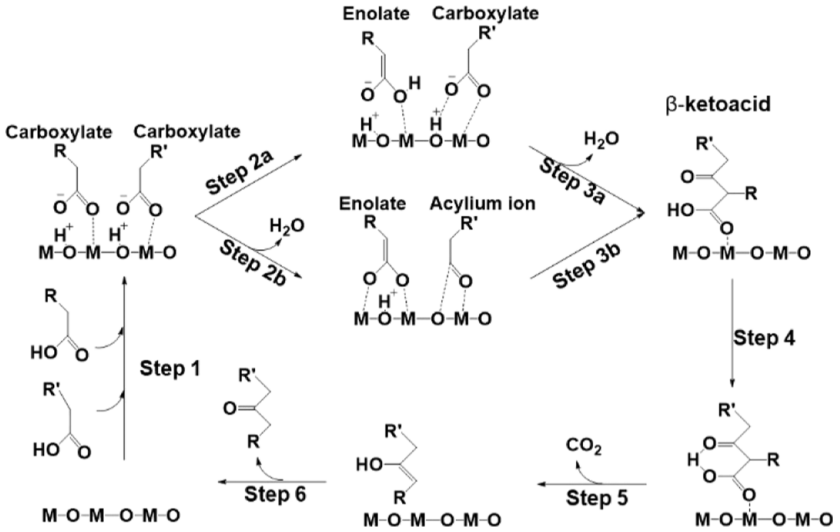

proposed route, an adjacent carboxylate directly attacks the enolate (step 3a) to form β-ketoacid,[10,12,15,17] whereas, in another proposed route, the dissociation of OH (step 2b) transforms the adjacent carboxylic acid into an acylium ion, which then attacks the enolate (step 3b) to form β-ketoacid.[14,18] The β-ketoacid formation upon C−C coupling was found to be the kinetically relevant step.[12] The tautomerization (step 4) of β-ketoacid followed by decarboxylation (step 5) releases CO_2 and forms an enol intermediate, which tautomerizes to the ketone product (step 6).

In these mechanisms, the carboxylates are the active intermediates for ketonization. There are still some debates remaining with regard to the configuration of the active carboxylate species because the carboxylates can bind by one or two oxygen atoms binding to the metal cations with three possible coordination structures, namely, monodentate, bridging bidentate, and chelating bidentate, as shown in Figure 1. Many previous works have proposed that bidentate

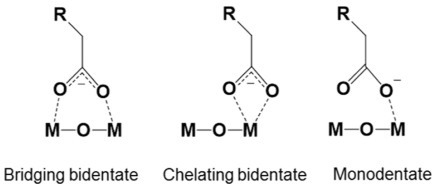

Figure 1. Different adsorption configurations of carboxylates on the metal oxide surface.

carboxylate is the intermediate for ketonization.[10,11,14,19,20] However, Wang and Iglesia[12,13] showed that for carboxylic acid ketonization on metal oxides, including TiO_2 and ZrO_2, monodentate carboxylates act as precursors to reactive enolate intermediates, while strongly bound bridging bidentate carboxylates are unreactive spectators. These works concluded that monodentate acetate species predominate on anatase TiO_2 and act as reactive intermediates in ketonization turnovers, whereas bidentate acetate species prevail on rutile TiO_2 but are not involved in ketonization turnovers, leading to the lower ketonization activity on rutile TiO_2 (523 K). However, a recent work by Fufachev et al.[21] showed that under elevated temperatures (598−698 K), bidentate species can also be activated for the ketonization reaction. At such high temperatures, the rutile TiO_2, which is predominated by bidentate species, becomes more active than anatase TiO_2 which has both mono- and bidentate species.

Most of the mechanisms or reaction intermediates are proposed based on Lewis acid−base site pairs on a clean metal oxide surface. However, the surfaces of metal oxides are often populated with hydroxyl groups which are generated upon dissociated adsorption of H_2O.[22−26] The role of surface hydroxyl groups in the catalysis of carboxylic acid ketonization on metal oxides has not been well understood. Water, either ubiquitous from biomass feedstocks, produced during the reaction, or used as a reaction medium, is always present in the catalytic process of biomass conversion, but few studies address the catalytic consequences of water on ketonization reactions. Pham et al.[10] studied the kinetics of acetic acid ketonization on Ru/TiO_2 catalysts and found that the reaction order is −0.1 for H_2O. They simply ascribed it to the competitive adsorption of H_2O with carboxylic acid on Ti cation sites. Boekaerts et al.[6] reported that the presence of H_2O inhibits the liquid-phase fatty acid ketonization catalyzed by TiO_2 (reaction order on H_2O is −0.16). It was proposed that such an inhibition effect could be caused by the competitive adsorption and/or participation of H_2O in reversible elementary steps. Lu and coworkers[27] also showed that the introduction of H_2O decreased the rate of acetic acid ketonization on $Ce_{1-x}Ti_xO_{2-\delta}$ mixed-oxide catalysts. They attributed this activity decline to the hydrolyzation of surface intermediates, such as β-ketoacids. In addition, the dissociative adsorption of H_2O introduces hydroxyl groups onto the surface, which is competitive with acetic acid conversion, and may also cause a decline in activity.

In this work, we used acetic acid and propanoic acid as model compounds to elucidate the effects of H_2O on the gas-phase ketonization activity over P25 TiO_2 catalysts, which well represents the anatase TiO_2 since the rutile phase only contributes to <2.5% of the overall ketonization activity of P25 TiO_2. Our kinetic measurement showed that adding H_2O vapor not only decreases the rate but also increases the intrinsic activation barrier of the carboxylic acid ketonization

https://doi.org/10.1021/jacs.2c08511
J. Am. Chem. Soc. 2023, 145, 99−109

reaction on TiO_2. By combining approaches of nuclear magnetic resonance spectroscopy (NMR) and diffuse reflectance infrared Fourier transform spectroscopy (DRIFTS), we demonstrated that there are multiple species present on the TiO_2 surface upon carboxylic acid adsorption, including molecular carboxylic acid, monodentate carboxylate, and chelating/bridging bidentate carboxylates. The presence of H_2O vapor increases the coverage of the less reactive bridging bidentate carboxylate associated with the adsorbed H_2O molecule, leading to a lower ketonization activity on hydrated TiO_2. Surface hydroxyl groups, which are consumed by interaction with carboxylic acid upon the formation of surface acetate species, do not impact the ketonization reaction.

2. EXPERIMENTAL SECTION

2.1. Materials. Commercial TiO_2 (P25, Sigma-Aldrich, 99.5%, surface area 55 m^2 g^{-1}) was used as the catalyst for acetic acid ketonization. The catalyst sample was calcined in static air at 823 K for 4 h before using for characterization or rate measurements. P25 TiO_2 is a $TiCl_4$ flame hydrolysis product. It consists of a physical mixture of ~75 wt % anatase phase and ~25 wt % rutile phase.[28,29] The predominant anatase phase was confirmed by X-ray diffraction (Figure S1). In addition, the anatase phase in P25 TiO_2 has a much smaller crystalline size than the rutile phase, and it was estimated that, in P25 TiO_2, the anatase phase has a 10-fold higher surface area than the rutile phase.[29] On the other hand, the rutile phase has a much lower catalytic activity for carboxylic acid ketonization, as previously reported by Wang and Iglesia[12] In this work, our measurement showed that a pure anatase TiO_2 sample has a 4-fold higher specific ketonization rate at 543 K than a pure rutile TiO_2 sample (Figure S2). Therefore, considering the differences in the surface area and specific ketonization rate between the anatase and rutile phases, it is estimated that the rutile phase only contributes to <2.5% of the overall ketonization activity of P25 TiO_2, which makes P25 TiO_2 well represent the anatase TiO_2 for the ketonization reaction.

2.2. Acetic Acid Ketonization Test. Acetic acid ketonization was studied using two methods: (1) temperature-programmed desorption (TPD) and (2) isothermal steady-state kinetic measurements. These tests were conducted in a fixed-bed quartz reactor (10 mm inner diameter) with plug-flow fluid dynamics. The reactor was placed within a resistively heated furnace with its temperature controlled by a digital feedback controller (Omega, CN3251). Inside the quartz reactor, the catalysts were supported on a coarse quartz frit and the bed temperature was recorded using a K-type thermocouple placed at the center of the catalyst bed. The reactant, acetic acid (Sigma-Aldrich, >99.9%), and H_2O were, respectively, introduced into vaporization zones located upstream of the reactor through gas-tight syringes (Hamilton, model 1002, 2.5 mL), mounted on syringe infusion pumps (KD Scientific, model 100). The vaporization zones were heated to 363 K (for acetic acid) and 358 K (for H_2O), respectively, allowing the fed liquids to evaporate in the carrier gas He (100 cm^3 min^{-1}). The respective partial pressures of acetic acid or H_2O were adjusted by controlling the liquid injection rates of the syringe infusion pumps. The mixture was fed to the reactor via heated transfer lines held at 473 K. The effluent stream was kept above 473 K and quantified with an online gas chromatograph (Agilent, 7890A) equipped with a capillary column (Agilent HP-1 19091Z-433, 30 m, 0.25 mm ID, 0.25 μm film) connected to a flame ionization detector.

For the acetic acid TPD, about 100 mg of a TiO_2 catalyst was used. The catalysts were pretreated by heating them to 823 K (5 K min^{-1}) in flowing air (50 cm^3 min^{-1}, zero grade) and holding for 1 h, before cooling to 393 K in flowing He (100 cm^3 min^{-1}, ultrahigh-purity grade) for acetic acid adsorption which was performed by flowing 1% acetic acid/He (50 cm^3 min^{-1}) for 10 min, followed by He purge (50 cm^3 min^{-1}) for 1 h. Then, the desorption procedure was conducted by heating the catalysts to 823 K (5 K min^{-1}) in flowing He (25 cm^3 min^{-1}), and the desorbed species in the effluent were quantified using a gas chromatograph in a 2 min interval. The TPD test of the hydrated TiO_2 was performed by a similar procedure, except that 3 kPa H_2O was introduced during the whole process of adsorption, purge, and desorption.

For the isothermal steady-state kinetic measurements, the TiO_2 catalysts were pressed, crushed, and sieved to retain 180−250 μm particles for the rate measurement. 10−25 mg of catalyst particles were mixed with 200 mg of SiC (200 mesh, Sigma-Aldrich) and loaded into the reactor. The catalysts were pretreated by heating them to the reaction temperature (513−543 K) in flowing He (100 cm^3 min^{-1}) and holding for 30 min. Then, the reactant gas mixture flow (100 cm^3 min^{-1}) with specific acetic acid and H_2O pressures was introduced into the reactor. The species in the effluent stream were quantified using the gas chromatograph in a 10 min interval. The rate measurements were performed under differential conditions with conversions lower than 10%.

The number of Lewis-acid sites on the TiO_2 catalyst was determined by the TPD of pyridine (pyridine-TPD), which was conducted following a procedure similar to acetic acid TPD, using about 100 mg of catalysts. The adsorption of pyridine was performed at 453 K by flowing 0.2 kPa of pyridine (in 50 cm^3 min^{-1} of He) for 30 min, followed by purging with He (100 cm^3 min^{-1}) for 2 h. Afterward, the sample was heated to 823 K (5 K min^{-1}) in flowing He (50 cm^3 min^{-1}), and the desorbed pyridine in the effluent was quantified using the gas chromatograph in a 3 min interval.

2.3. Infrared Spectroscopic Studies of the Acetic Acid Reaction on TiO_2. The DRIFTS studies of the adsorption and TPD of acetic acid on TiO_2 catalysts were performed on a Nicolet iS50R FT-IR spectrometer (Thermo Scientific) equipped with a liquid nitrogen-cooled MCT detector and a Praying Mantis diffuse reflection accessory (Harrick Scientific Products Inc.). To prevent acetic acid from condensing, all the gas lines were heated to 373 K and the sample cell was heated to 373 K using hot H_2O recirculation. Before the measurement, the background spectra were collected using KBr powder under flowing He (10 mL min^{-1}) at temperatures of 393, 423, 473, 523, 573, 623, 673, 723, and 773 K, respectively, and used as the backgrounds for the spectra collected at the same temperatures. The catalyst powders placed in the sample cell were pretreated by heating to 773 K and holding for 30 min, followed by cooling down to 393 K in flowing He (20 mL min^{-1}). For the acetic acid adsorption at 393 K, about 2 μL of acetic acid was dosed into the heated injection port (373 K) upstream, where the acetic acid was vaporized and carried by flowing He (20 mL min^{-1}) into the sample cell. After acetic acid adsorption, the catalysts were purged by flowing He (20 mL min^{-1}) for 40 min before ramping up for desorption. The TPD was performed by heating the sample at 10 K min^{-1} and holding it at each measurement temperature for 1 min for spectrum collection. The experiment of hydrated TiO_2 was conducted using the same procedure, except that during the whole process of acetic acid adsorption and desorption, about 2 kPa of H_2O was introduced into the carrier gas He (20 mL min^{-1}) by passing through a bubbler containing DI H_2O at room temperature.

2.4. NMR Spectroscopic Studies of Acetic Acid Adsorption on TiO_2. In situ ^1H and ^{13}C magic angle spinning (MAS) NMR spectroscopy measurements were conducted on a Varian-Agilent Inova wide-bore 300 MHz NMR spectrometer using a commercial 7.5 mm ceramic pencil-type MAS probe operating at ^{13}C and ^1H Larmor frequencies of 75.430 and 299.969 MHz, respectively. Samples were rotated at the magic angle, spinning at ~3.8 kHz. Single-pulse ^1H (^{13}C) sequences consists of a $\pi/4$ pulse width of 2.25 μs (3.5 μs), an acquisition time of 340 ms (400 ms), and a recycle delay of 5 s (10 s). $^1H-^{13}C$ cross-polarization (CP) MAS NMR spectra were acquired by a 5 μs proton excitation followed by a 2.1 ms contact time. The acquisition occurred over 50 ms, and a 2 s recycle delay was employed. All spectra were externally referenced to adamantane at 1.82 and 38.48 ppm for ^1H and ^{13}C, respectively.

Sample integrity was maintained by utilizing sealed, high-temperature, and high-pressure MAS NMR rotors for sample preparation and analysis.[30−33] The adsorption of 1−^{13}C acetic acid on dry and hydrated TiO_2 catalysts (~130 mg) was conducted with the approach used in TPD experiments (Section 2.2) under similar pretreatment,

https://doi.org/10.1021/jacs.2c08511
J. Am. Chem. Soc. 2023, 145, 99−109

adsorption, and purging conditions. Multilayer coverage experiments were conducted by pretreating a sample as described above and directly injecting the desired quantity of 50% 1−^{13}C acetic acid into the NMR rotor with a microsyringe.

2.5. Computational Modeling of the NMR Chemical Shifts. Computational modeling of the NMR chemical shifts was carried out using the Amsterdam Density Functional (ADF-2017.113) package. Geometries were optimized using the generalized gradient approximation (GGA) with Grimme's third-generation dispersion correction applied to the Becke−Lee−Yang−Parr functional (GGA: BLYP-D3).[34−36] The calculations were conducted using the Slater-type all-electron, triple-ζ, 2-polarization function (TZ2P) basis set.[37]^{13}C NMR calculations were performed on the geometry-optimized structures at the same level of the theory to evaluate the chemical shielding for each atom. To convert the calculated shielding to the experimentally observed scale with reference to adamantane (38.48 ppm), the following equation is used: $\delta_{obs} = 134.3276 - \delta_{calc} + 38.48$. Our titania surface models previously described and employed were repurposed for this study.[38]

3. RESULTS AND DISCUSSION

3.1. Configuration of Acetic Acid Adsorption on TiO_2 Identified DRIFTS. The surface species of acetic acid adsorption on TiO_2 catalysts and their reactivities were investigated using temperature-resolved DRIFTS. The dry TiO_2 catalysts were obtained by *in situ* pretreatment at 723 K in flowing He. Figure 2 shows the DRIFTS spectra of acetic acid adsorption on dry TiO_2 at 393 K and desorption at elevated temperatures. As shown in Figure 2a, on dry TiO_2 catalysts, the surface hydroxyl groups, including the terminal (3720 cm^{-1}) and bridging (3671 cm^{-1}) OH groups, cannot be completely removed (see Figure S3 in the Supporting Information for the DRIFTS spectra of catalyst pretreatment).

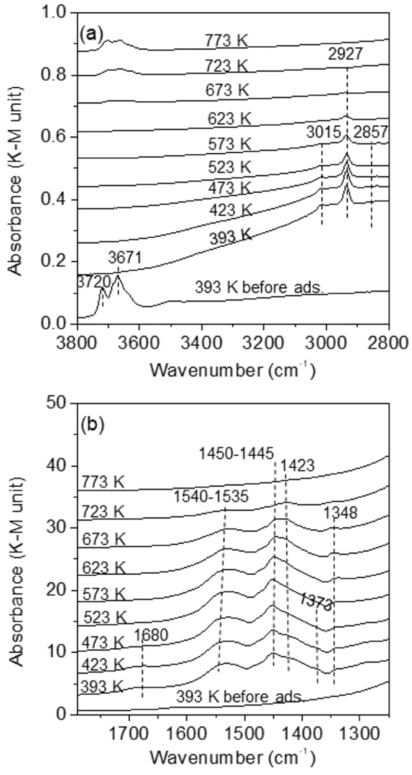

Figure 2. DRIFTS spectra of acetic acid TPD on dry TiO_2 in (a) 3800−2800 and (b) 1900−1200 cm^{-1} regions, respectively (acetic acid adsorption temperature 393 K).

However, after introducing acetic acid vapor at 393 K, these OH groups completely disappeared because of their consumption by the reaction with acetic acid forming an ester-like linkage.[39−41]

The adsorption of acetic acid on TiO_2 formed predominantly acetate species. The broad band at 1540−1535 cm^{-1} is ascribed to the asymmetric stretching [$\nu(OCO)_{as}$] of various acetates, whereas the bands at 1450−1445 cm^{-1} and the shoulder at 1423 cm^{-1} are assigned to the symmetric stretching [$\nu(OCO)_s$] of the chelating and bridging bidentate acetate species, respectively.[39,42−45] The weak band at 1378 cm^{-1} is assigned to the symmetric stretching [$\nu(OCO)_s$] of monodentate acetate.[12] Molecularly adsorbed acetic acid was also observed, as indicated by the stretching of carbonyl [ν(C═O)] at 1680 cm^{-1}.[39,44] The bands at 2857, 2927, and 3015 cm^{-1} are associated with the stretching vibration of the C−H bond [ν(C−H)]. The lower-frequency ones at 2857 and 2927 cm^{-1} are assigned to C−H on the alkyl group ($-CH_3$). The frequencies of these two bands remain the same as the acetic acid coverage changes, indicating that the adsorbed acetic acid species remain isolated as the C−H bonds are not perturbed by interactions between vicinal molecules. The higher-frequency one at 3015 cm^{-1} is assigned to the olefinic C−H bond (═C−H).[46] The presence of olefinic C−H is likely associated with the formation of enolate intermediates (Scheme 1). As the temperature increased, these surface species began to decrease upon the ketonization reaction. The bands for monodentate acetate and molecular acetic acid were the first to disappear at 473 K, indicating the higher activities of these species. The bidentate acetates were more stable and less reactive, being retained at much higher temperatures. It is worth noting that the disappearance of the surface acetate/acetic acid species is because of the ketonization reaction forming acetone instead of simply desorption, as shown by acetic acid TPD results in the following section (Figure 7). The stable bidentate species can eventually undergo a ketonization reaction at elevated temperatures, which was also confirmed by Fufachev et al.[21]

The reaction intermediates on hydrated TiO_2 were examined by continuously feeding H_2O vapor (~2 kPa) during the acetic acid adsorption and desorption process, as shown in Figure 3. The broad band at ~3400 cm^{-1} is assigned to the OH stretching of H-bonded H_2O molecules on the surface. Upon acetic acid adsorption, this broad H_2O band shifts to a lower frequency (~3100 cm^{-1}) due to the interaction between adsorbed H_2O molecules and surface acetic species. The presence of H_2O strongly affected the configuration of adsorbed acetic acid species on the TiO_2 surface. As shown in Figure 3b, the monodentate acetate (1373 cm^{-1}) was still present upon the hydration TiO_2, but the molecularly adsorbed acetic acid (1665 cm^{-1}) was absent. While the chelating bidentate acetate (1450−1445 cm^{-1}) was still one of the predominant species, a much higher shoulder band at 1416 cm^{-1} was observed on the hydrated TiO_2 surface in comparison to the 1422 cm^{-1} shoulder band for bridging bidentate acetate on dry TiO_2 (Figure 2b). Considering that it is unlikely that the presence of H_2O would facilitate an acetate species to bond to a second Ti site to form a bridging bidentate structure, we postulate that the 1416 cm^{-1} shoulder band on hydrated TiO_2 is likely related to a species associated with H_2O molecule(s). It has been previously reported that the adsorption of cyclohexanone on the hydrated anatase TiO_2(101) surface was impacted by physisorbed H_2O.[47] The

https://doi.org/10.1021/jacs.2c08511
J. Am. Chem. Soc. 2023, 145, 99−109

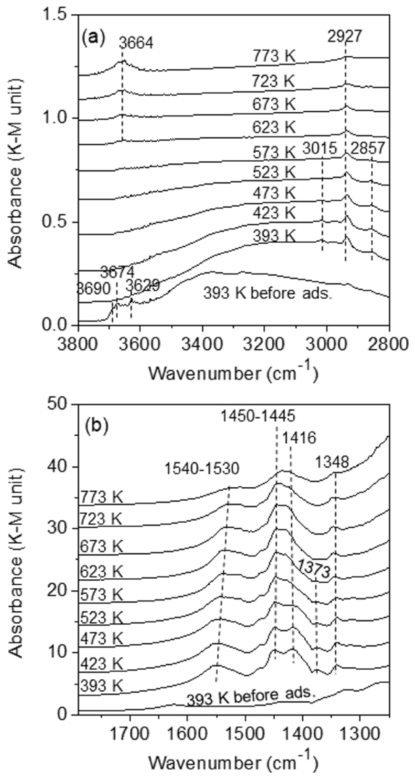

Figure 3. DRIFTS spectra of acetic acid TPD on the hydrated TiO_2 in (a) 3800−2800 and (b) 1900−1200 cm^{-1} regions, respectively (H_2O pressure = 2 kPa, acetic acid adsorption temperature 393 K).

physisorbed H_2O bridges the cyclohexanone carbonyl and the TiO_2 surface, increasing the cyclohexanone adsorption enthalpy (from 24 to 37 kJ mol^{-1}) and causing the red shift of the carbonyl IR band (from 1694 to 1681 cm^{-1}). Therefore, we propose the possible configurations of hydrated bridging bidentate acetate, with one of the carboxylic oxygens hydrogen-bonded to a physisorbed H_2O molecule, as shown in Scheme 2. These hydrated acetate species were likely derived from the molecularly adsorbed acetic acid (1665 cm^{-1}) and/or the chelating bidentate acetate (1450−1445 cm^{-1}) which either disappeared or decreased on the hydrated TiO_2. As the temperature increases, the more reactive monodentate acetate (1373 cm^{-1}) disappears first, while the less reactive

Scheme 2. Proposed configuration of Bridging Bidentate Acetate Species Formed on a Hydrated TiO_2 Surface

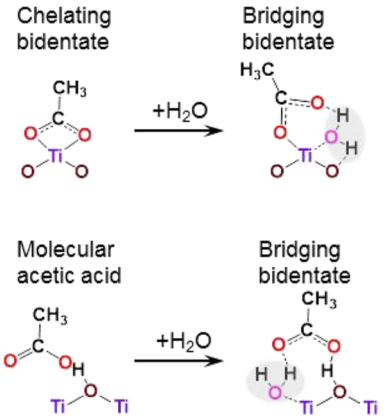

bidentate acetates (1416 and 1450−1445 cm^{-1}) are retained at higher temperatures, similar to the case of dry TiO_2.

Figure 4 shows the relative intensities of the acetate stretching bands [ν(OCO), 1600−1360cm^{-1}] as a function

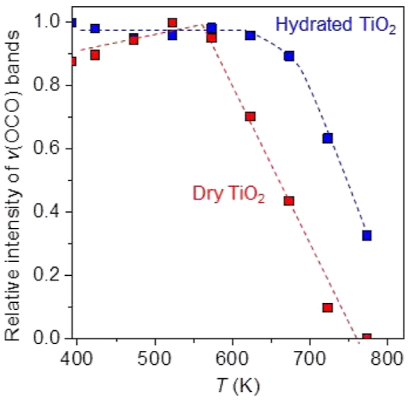

Figure 4. Relative total intensities of the acetate stretching bands [ν(OCO), 1600−1360 cm^{-1}] on the DRIFTS spectra in Figures 1 and 2 as a function of temperature (normalized by the initial intensity at 393 K).

of temperature. The higher acetate disappearance temperature for the hydrated TiO_2 indicates that the acetate species were less reactive on hydrated TiO_2 than on dry TiO_2.

3.2. Configuration of Acetic Acid Adsorption on TiO_2 Identified by In Situ MAS NMR. The configurations of acetic acid adsorption on dry and hydrated TiO_2 surfaces were further identified using *in situ* solid-state ^1H and ^{13}C MAS NMR. The adsorption of one monolayer of 1−^{13}C acetic acid on TiO_2 was conducted in a plug-flow reactor at 393 K before transferring the TiO_2 sample to the NMR rotor under the protection of the N_2 atmosphere. Prior to the acetic acid adsorption, the dry TiO_2 catalyst was obtained by *in situ* pretreatment at 823 K in flowing He for 30 min. For the case of hydrated TiO_2, after 823 K pretreatment and then cooling to 393 K, H_2O vapor (~3 kPa) was continuously fed before, during, and after the process of acetic acid adsorption.

The configurations of surface H_2O molecules and OH groups were probed via *in situ* solid-state MAS ^1H NMR, as shown in Figure 5. Dry TiO_2 contains bridging OH (4.5 ppm at 393 K[48]) (Figure 5a), which disappeared upon acetic acid

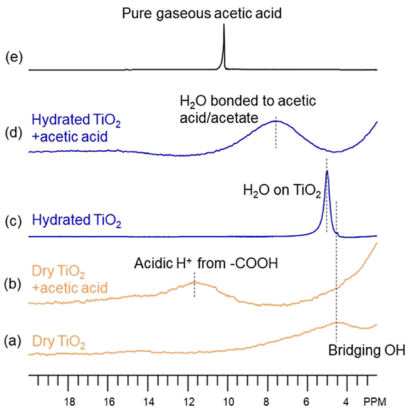

Figure 5. ^1H MAS NMR spectra for (a,b) dry TiO_2 before and after acetic acid adsorption, (c,d) hydrated TiO_2 before and after acetic acid adsorption, and (e) pure gaseous acetic acid (393 K).

https://doi.org/10.1021/jacs.2c08511
J. Am. Chem. Soc. 2023, 145, 99−109

adsorption (Figure 5b), consistent with the DRIFTS result (Figure 2). A peak at 11.6 ppm is assigned to the acidic proton from acetic acid (Figure 5b). Compared to pure acetic acid at 393 K where the acidic proton resonates at 10.2 ppm (Figure 5e),[49] acetic acid on TiO_2 shows a peak at 11.6 ppm, indicating a strong electronic interaction with the TiO_2 surface. The hydrated TiO_2 surface (Figure 5c) is dominated by a signal from molecularly adsorbed H_2O (4.9 ppm at 393 K).[50,51] After acetic acid adsorption (Figure 5d), the 4.9 ppm peak shifted to 7.6 ppm, indicating that the coadsorption of acetic acid and H_2O significantly changed the configuration of surface H_2O species. Based on the drastic downfield shifting of the H_2O peak in the presence of acetic acid, it is evident that the H_2O molecule is bonded to surface acetic acid or acetate species and deshielded through interaction with acetic acid, as proposed in Scheme 2.

The configurations of the carboxylic group of the surface acetic acid or acetate species on both dry and hydrated TiO_2 surfaces were studied via *in situ* surface-sensitive ^{13}C CP MAS NMR spectra, as shown in Figure 6. These CP MAS spectra

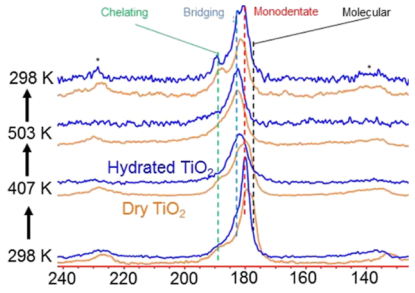

Figure 6. $^{1}H-^{13}C$ CP MAS NMR of acetic acid adsorption on dry and hydrated TiO_2 at 298, 407, and 503 K, respectively (* indicates spinning side bands).

represent carbon species present on the TiO_2 surface whose molecular motion is restricted due to the interaction with the surface functional groups. The spectra illustrate an array of species assigned as molecularly adsorbed acetic acid (ca. 177.5 ppm), monodentate acetate (ca. 179.8 ppm), bridging bidentate acetate (ca. 182.5 ppm), and chelating bidentate acetate (ca. 188.1 ppm). The assignment of surface acetate species was made through a combination of literature, experimental, and computational insights. It was reported for organometallic Zn complexes that chelating bidentate acetates would resonate most downfield at 184 ppm and monodentate acetate would be found at 176 ppm.[52] Bridging bidentate acetates are in a geometric configuration which is a hybrid between the monodentate acetate and chelating acetate binding modes and exhibited a chemical shift between the two at 179 ppm. Indeed, these speculated assignments from organometallic literature are in good agreement with the trends outlined by our theoretical calculations of acetic acid adsorption modes on anatase TiO_2 (Table 1). The calculations indeed predict molecularly adsorbed acetic acid at the lowest chemical shift (186 ppm), increasing to 187 ppm for monodentate acetate, 188 ppm for bridging bidentate acetate, and 198 ppm for chelating bidentate acetate. The trend shown above is a reasonable agreement with experimentally observed trends, validating the peak assignments.

To further confirm the assignments, an excess of acetic acid was applied to the dry TiO_2 sample (Figure S6). Under conditions exceeding the monolayer, an increased abundance of molecularly adsorbed acetic acid is expected to be visible from the CP experiment. Note that liquid-phase acetic acid would not be visible in CP NMR. Indeed, only a relatively small increase in signal is observed when such a large excess of acetic acid is applied. It is clear from the six-monolayer coverage spectrum that the most shielded signal (177.5 ppm) is enhanced. This confirms the assignment of this signal as the molecular species.

At 298 K, the dry TiO_2 exhibits more molecular and chelating species than the hydrated catalyst which relatively favors bridging and monodentate configurations. At elevated temperatures (407 K), the up-field signals become suppressed in both the dry and hydrated TiO_2, favoring bridging species which persist up to 503 K. At this temperature, the species are likely more mobile, which suppresses all signals except those very tightly bound (i.e. bridging). The magnitude of the temperature-induced chemical shift is again inconsistent with what is expected from thermal perturbation, evidenced by enhanced shielding (Figures S3 and S4) and solidifying the identity of acetate species that are tightly bound to the surface.[50] At room temperature, three binding modes can be resolved: chelating, bridging, and monodentate. Molecular species may be present but are low in abundance after the heating. Inconsistencies between the initial and final state of the acetate species at 298 K can be explained by the reactivity of the catalysts, evidenced by the formation of CO_2 (125.5 ppm) and other reaction products (Figure S7). Indeed, the magnitude of this conversion is higher in the case of the dry TiO_2 for the same time period, consistent with reactivity measurements of the dry TiO_2 exhibiting higher reaction rates. In this final condition, the molecular species have been exhausted, either as a product or converted to another surface species. Other species are similarly suppressed but to a smaller extent.

Table 1. NMR Chemical Shifts of Different Modes of Acetic Acid Adsorption on TiO_2 Determined by Experiments and DFT Calculation

Species	Molecular acetic acid	Monodentate acetate	Bridging bidentate acetate	Chelating bidentate acetate
Experimental	177.5 ppm	179.8 ppm	182.5 ppm	188.1 ppm
Calculation	186.26 ppm	187.4 ppm	188.14 ppm	198.09 ppm
Structure	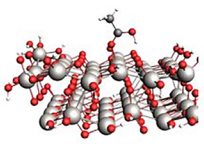	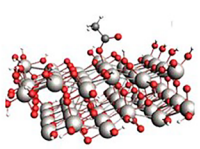	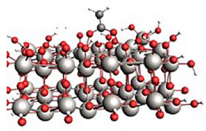	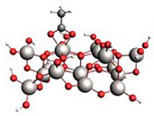

https://doi.org/10.1021/jacs.2c08511
J. Am. Chem. Soc. 2023, 145, 99−109

3.3. Acetic Acid TPD for Comparing the Activities of Adsorbed Intermediates on Dry and Hydrated TiO_2. The ketonization activities of the dry and hydrated TiO_2 catalysts were compared by TPD of adsorbed acetic acid (acetic acid TPD) conducted with the absence and presence of co-fed H_2O vapor (1.5 kPa), respectively, as shown in Figure 7. The acetic

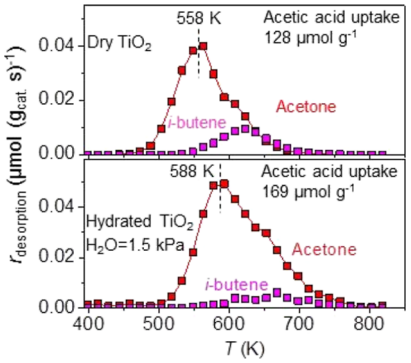

Figure 7. Profiles of acetic acid TPD on the dry and hydrated TiO_2 (acetic acid adsorption temperature 393 K).

acid uptake of the hydrated TiO_2 (169 μmol g^{-1}) was close to the number of Lewis acid sites determined by pyridine TPD (162 μmol g^{-1}) but that on dry TiO_2 was slightly lower (128 μmol g^{-1}). It was probably because some of the surface species on dry TiO_2 either desorbed or reacted during the 1 h of purging at 393 K, considering that the dry TiO_2 surface contained some weakly adsorbed species (e.g., molecular acetic acid, Figure 2), and it was also more reactive in catalyzing the reaction of surface species (Figures 4 and 5).

On both dry and hydrated catalysts, acetone, the product of acetic acid ketonization (reaction 1, Scheme 3), was the major

Scheme 3. Sequential Reactions of Acetic Acid on TiO_2

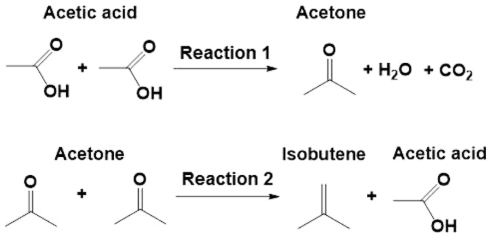

desorbed species. A small amount of isobutene resulting from acetone condensation followed by decomposition (reaction 2, Scheme 3)[53,54] was detected at a higher temperature (>550 K). No acetic acid was detected in TPD, indicating that all the adsorbed species underwent the ketonization reaction. Similar acetone formation during acetic acid TPD was previously reported on CaO.[55] The broadness of the desorption peak is likely due to both distribution of acid sites and the sharply reduced ketonization rate caused by decreasing coverage of acetic acid.

The product desorption temperature was higher on hydrated TiO_2 in the presence of H_2O vapor than on dry TiO_2 (588 vs 558 K), indicating that the hydrated TiO_2 surface is less reactive for ketonization, consistent with the DRIFTS results (Figure 4). However, when we prehydrated TiO_2 catalysts with 1.5 kPa H_2O at 393 K, followed by conducting acetic acid TPD in He without cofeeding H_2O vapor, the TPD profile looked similar to that of dry TiO_2 (see Figure S4 in the Supporting Information). This suggests that it is the molecular H_2O instead of the surface hydroxyl groups that cause activity decrease. Lower *i*-butene formation in the presence of co-fed H_2O suggests that H_2O also suppresses the secondary reaction of acetone, as also confirmed by the test of acetone reaction on TiO_2 catalysts (Figure S5 in the Supporting Information).

3.4. Kinetic Consequences of H_2O on Carboxylic Acid Ketonization on TiO_2. The rates of acetic acid ketonization on TiO_2 catalysts were measured in the temperature range of 513−553 K. Ketonization of acetic acid (reaction 1, Scheme 3) formed acetone as the major product. The secondary reaction of acetone via aldol condensation followed by decomposition led to the formation of isobutene (reaction 2, Scheme 3). This secondary acetone reaction occurred at a low carbon selectivity (<10%, Figure S8) because the active sites, namely, the Lewis acid−base site pairs, were predominantly occupied by the strongly adsorbed acetic acids. Negligible catalyst deactivation was observed during the reaction test (Figure S9). We performed temperature-programmed oxidation of the spent catalysts (after acetic acid reactions without co-fed H_2O) to investigate the surface carbon deposition (Figure S10), which shows that the coke formation was negligible.

Parallel to the ketonization pathway, acetic acid underwent dehydration, forming acetic anhydride, which was an equilibrium-limited reaction. Therefore, acetic acid and acetic anhydride were treated as a reactant lump, in which acetic acid was the predominant component, as the acid-to-anhydride ratio varied from ∼160 to ∼5000 depending on the temperature and H_2O partial pressure.

The presence of H_2O vapor led to the decrease of ketonization activity on TiO_2. Figure 8a shows the rate of acetic acid ketonization, $r_{Ketonization}$, as a function of acetic acid pressure, P_{Acetic}. When H_2O was not co-fed, $r_{Ketonization}$ increased with P_{Acetic}, following a typical Langmuir−Hinshelwood kinetic model and reached the maximum when acetic acid saturated the catalyst surface at 5 kPa. Such kinetic dependence is similar to the previous report by Wang and Iglesia.[12,13] However, further increasing P_{Acetic} to 12 kPa, instead of maintaining a constant $r_{Ketonization}$, led to a slight decrease in $r_{Ketonization}$. The slight decrease of ketonization activity was likely caused by the increasing H_2O pressure (P_{H_2O}, up to ∼0.05 kPa) as the increasing P_{Acetic} moved the acid−anhydride equilibrium to the anhydride side and thus increased the H_2O pressure.

When cofeeding 0.5 kPa of H_2O, the ketonization rate was markedly decreased by half in comparison to that without H_2O cofeeding. However, further increasing P_{H_2O} to 1, 2, and 3.8 kPa did not result in further activity decline. The inhibition effect of water is reversible. Upon stopping H_2O cofeeding, the ketonization rate can be fully restored (Figure S9), which rules out the water-induced changes in the catalyst including phase change under this reaction condition as phase transformation of anatase typically requires a temperature near 900 K.[56,57] Also, it is noted that the acetic acid coverage always reached saturation at around 5 kPa, regardless of H_2O pressure (0−1 kPa). These results ruled out the adsorption competition between H_2O and acetic acid because, otherwise, a higher acetic acid pressure would be required to saturate the catalyst surface when H_2O pressure increased. This is also consistent with the similar acetic uptake on TiO_2 with and without H_2O vapor measured by TPD.

https://doi.org/10.1021/jacs.2c08511
J. Am. Chem. Soc. 2023, 145, 99−109

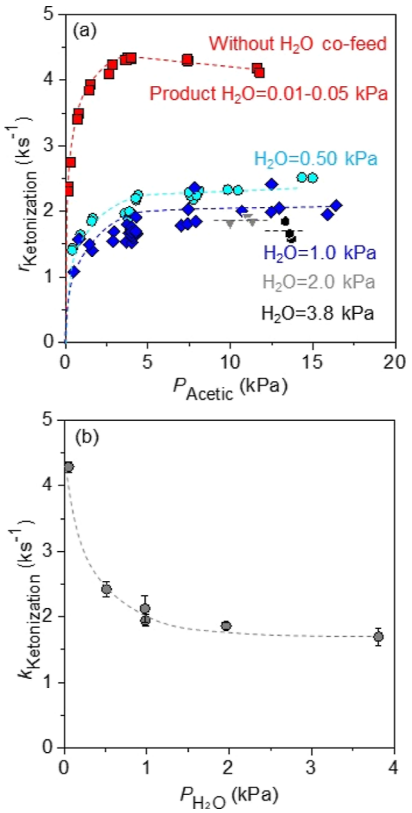

Figure 8. (a) Rates of acetic acid ketonization ($r_{Ketonization}$) on TiO_2 catalysts (543 K) as a function of acetic acid pressure (P_{Acetic}) under various constant H_2O pressures (0.05−3.8 kPa); (b) effective rate constant ($k_{Ketonization}$) for acetic acid ketonization (543 K) as a function of H_2O partial pressure (P_{H_2O}).

Wang and Iglesia[12] have previously demonstrated that the β-ketoacid formation upon C−C coupling (step 3a or 3b, Scheme 1) instead of the enolate formation upon α-C−H cleavage (step 2a or 2b, Scheme 1) is the kinetically relevant step for carboxylic acid ketonization, as confirmed by the weak kinetic isotope effect (KIE) of deuterated reactants (KIE value 1.1). We also observed similar close-to-unity KIE values (1.12−1.22) for both acetic acid and propanoic acid, as shown in Table 2, confirming that the formation or cleavage of bonds containing a H-atom is not involved in the kinetically relevant step. In addition, on both the dry and hydrated TiO_2 surfaces, the deuterated acetic acid presented a consistent weak KIE, indicating that the presence of H_2O vapor did not alter the kinetic relevance of the C−C coupling step.

Because H_2O neither competes with acetic acid adsorption nor influences the kinetically relevant step, the ketonization reactions on the dry and hydrated surfaces share the same Langmuir−Hinshelwood kinetic model, in which acetic acid is the only adsorption intermediate, as expressed by eq 2

$$r_{Ketonization} = \frac{k_{Ketonization}(K_{Ads}P_{Acetic})^2}{(1 + K_{Ads}P_{Acetic})^2} \quad (2)$$

where K_{Ads} represents the adsorption equilibrium constant and $k_{Ketonization}$ is the effective rate constant for the combined enolation and C−C coupling steps. On an acetic acid-saturated surface ($K_{Ads}P_{Acetic} \gg 1$), eq 2 is simplified to a zeroth-order rate expression

$$r_{Ketonization} = k_{Ketonization} \quad (3)$$

where $k_{Ketonization}$ is the apparent zeroth-order rate constant.

Figure 8b shows the apparent zeroth-order rate constant $k_{Ketonization}$ as a function of H_2O partial pressure P_{H_2O}. The presence of H_2O vapor markedly suppressed the ketonization activity on TiO_2, but this suppression effect leveled out as the H_2O pressure increased to ~1 kPa. We speculate that H_2O hydrated the TiO_2 surface and modified the Lewis-acid site pairs and/or adsorption of acetic acid or intermediates, which led to the decrease in the ketonization activity. This explains the phenomenon observed on the dry TiO_2 catalyst that after acetic acid saturated the surface at 5 kPa, further increasing P_{Acetic} started to decrease the ketonization rate (Figure 8a). It can be ascribed to the hydration of the TiO_2 surface by the small amount of H_2O (<0.05 kPa), of which partial pressure (P_{H_2O}) increased with P_{Acetic} according to the acid−anhydride equilibrium. When cofeeding extra H_2O, the extent of surface hydration reached a maximum under a P_{H_2O} of 1 kPa; thus, further increasing P_{H_2O} did not further influence the activity.

Figure 9a shows the Arrhenius plots for the zeroth-order rate constants of acetic acid ketonization on dry (without H_2O cofeeding) and hydrated TiO_2 catalysts (upon cofeeding 2 kPa of H_2O), respectively. The presence of H_2O (2 kPa) not only decreased the rate constant but also increased the apparent activation energy from 127 ± 1 kJ mol^{-1} on dry TiO_2 to 150 ± 2 kJ mol^{-1} on hydrated TiO_2. A similar trend was also observed for propanoic acid ketonization (Figure 9b), with the apparent activation energy increasing from 111 ± 4 kJ mol^{-1} on dry TiO_2 to 134 ± 7 kJ mol^{-1} on hydrated TiO_2. These changes in activation energies further indicate that the decrease in ketonization activity upon cofeeding H_2O is not caused by competitive adsorption of H_2O but due to modification of the active sites or reaction mechanism by H_2O.

Both NMR and DRIFTS results consistently confirm that there are multiple types of intermediates formed on the TiO_2 surface upon acetic acid adsorption. The dry TiO_2 surface contains four types of species, including molecular acetic acid, monodentate acetate, chelating bidentate acetate, and bridging bidentate acetate, among which the chelating bidentate acetate predominates. On the hydrated TiO_2 surface, all three types of acetate species were observed, with the absence of molecular acetic acid. The hydrated TiO_2 surface contains a higher amount of bridging bidentate acetate species, which are associated with physisorbed H_2O molecules hydrogen-bonded on the TiO_2 surface. The evolution of these species with

Table 2. KIE of Deuterated Carboxylic Acid on the Ketonization Reaction

carboxylic acid reactant	temperature (K)	H_2O cofeeding	$r_{Ketonization,H}/r_{Ketonization,D}$ ratio (KIE value)
CH_3COOH/CD_3COOD(6 kPa)	543	0	1.12
	543	2 kPa	1.16
C_2H_5COOH/C_2D_5COOD(3 kPa)	533	0	1.22

https://doi.org/10.1021/jacs.2c08511
J. Am. Chem. Soc. 2023, 145, 99−109

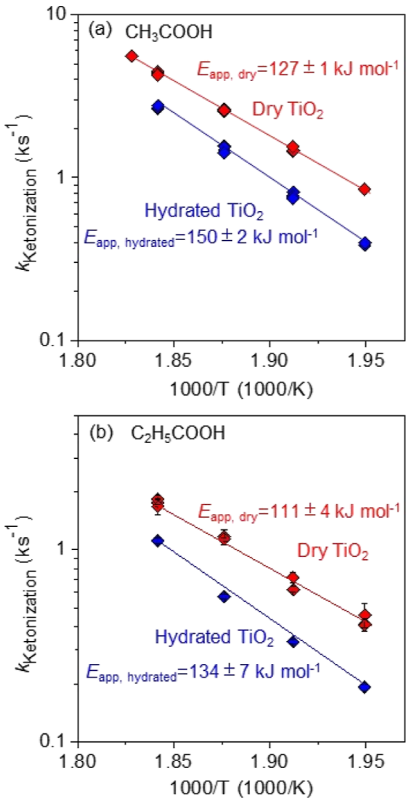

Figure 9. Arrhenius plots for zeroth-order rate constants of (a) acetic acid and (b) propanoic acid ketonization on dry (without H_2O cofeeding) and hydrated (P_{H_2O} = 2 kPa) TiO_2, respectively.

temperature suggests a reactivity order of bridging bidentate acetate < chelating bidentate acetate < monodentate acetate ≈ molecular acetic acid. Therefore, the hydrated TiO_2 surface which is more populated with the less reactive bridging bidentate acetate species is less reactive in catalyzing carboxylic acid ketonization, as confirmed by kinetic measurements.

4. CONCLUSIONS

In this work, the effects of H_2O on the carboxylic acid ketonization reaction were examined by NMR, DRIFTS, and kinetic measurements. P25 TiO_2 was used as a model anatase TiO_2 catalyst since the rutile phase only contributes to <2.5% of the overall ketonization activity of P25 TiO_2. The adsorption of carboxylic acid on the dry TiO_2 forms four types of surface species, including molecular carboxylic acid, monodentate carboxylate, chelating bidentate carboxylate, and bridging bidentate carboxylate. The chelating bidentate carboxylate is the predominant species. The presence of H_2O vapor impacts the configuration of carboxylic acid adsorption species on the TiO_2 surface. On the hydrated TiO_2, all three types of acetate species were observed, without the molecularly adsorbed carboxylic acid. The hydrated TiO_2 surface contains a higher amount of bridging bidentate carboxylate species associated with physisorbed H_2O molecules hydrogen-bonded on the TiO_2 surface. The reactivities of these four types of surface species follow the order bridging bidentate carboxylate < chelating bidentate carboxylate < monodentate carboxylate ≈ molecular carboxylic acid. The hydrated anatase TiO_2 surface forms a higher fraction of the more stable bridging bidentate carboxylate, in comparison to the dry TiO_2 surface, leading to the lower ketonization reactivity of the hydrated TiO_2.

■ ASSOCIATED CONTENT

Supporting Information

The Supporting Information is available free of charge at https://pubs.acs.org/doi/10.1021/jacs.2c08511.

DRIFTS spectra, acetic acid TPD profiles, and NMR spectra (PDF)

■ AUTHOR INFORMATION

Corresponding Authors

Jian Zhi Hu − *Institute for Integrated Catalysis, Pacific Northwest National Laboratory, Richland, Washington 99354, United States; The Gene and Linda Voiland School of Chemical Engineering and Bioengineering, Washington State University, Pullman, Washington 99164, United States;* orcid.org/0000-0001-8879-747X; Email: Jianzhi.Hu@pnnl.gov

Huamin Wang − *Institute for Integrated Catalysis, Pacific Northwest National Laboratory, Richland, Washington 99354, United States;* orcid.org/0000-0002-3036-2649; Email: Huamin.Wang@pnnl.gov

Yong Wang − *Institute for Integrated Catalysis, Pacific Northwest National Laboratory, Richland, Washington 99354, United States; The Gene and Linda Voiland School of Chemical Engineering and Bioengineering, Washington State University, Pullman, Washington 99164, United States;* orcid.org/0000-0002-8460-7410; Email: Yong.Wang@pnnl.gov

Authors

Fan Lin − *Institute for Integrated Catalysis, Pacific Northwest National Laboratory, Richland, Washington 99354, United States*

Wenda Hu − *Institute for Integrated Catalysis, Pacific Northwest National Laboratory, Richland, Washington 99354, United States; The Gene and Linda Voiland School of Chemical Engineering and Bioengineering, Washington State University, Pullman, Washington 99164, United States*

Nicholas R. Jaegers − *Institute for Integrated Catalysis, Pacific Northwest National Laboratory, Richland, Washington 99354, United States; The Gene and Linda Voiland School of Chemical Engineering and Bioengineering, Washington State University, Pullman, Washington 99164, United States*

Feng Gao − *Institute for Integrated Catalysis, Pacific Northwest National Laboratory, Richland, Washington 99354, United States;* orcid.org/0000-0002-8450-3419

Complete contact information is available at: https://pubs.acs.org/10.1021/jacs.2c08511

Author Contributions

F.L. and W.H. contributed equally. The manuscript was written with the contributions of all authors. All authors have approved the final version of the manuscript.

Funding

The U.S. Department of Energy (DOE), Office of Basic Energy Sciences, Division of Chemical Sciences, Geosciences, and Biosciences. The U.S. Department of Energy (DOE), Office of Energy Efficiency and Renewable Energy (EERE), and Bioenergy Technologies Office (BETO).

Notes

The authors declare no competing financial interest.

■ ACKNOWLEDGMENTS

This work was primarily supported by the U.S. Department of Energy (DOE), Office of Science (SC), Basic Energy Sciences (BES), Division of Chemical Sciences, Geosciences, and Biosciences within the Catalysis Science program (DE-AC05-RL01830, FWP-47319) and carried out at the Pacific Northwest National Laboratory (PNNL), a multiprogram national laboratory operated for the DOE by Battelle. F.L. and H.W. were also partly supported by the U.S. Department of Energy (DOE), Office of Energy Efficiency and Renewable Energy (EERE), and Bioenergy Technologies Office (BETO) for this work. W.H. is also partly supported by Chambroad Scholarship for pursuing his Ph.D. Part of the work was conducted in the William R. Wiley Environmental Molecular Sciences Laboratory (EMSL), a national scientific user facility sponsored by DOE's Office of Biological and Environmental Research and located at the PNNL. Computing time was granted by a user proposal at the EMSL and the National Energy Research Scientific Computing Center (NERSC).

■ REFERENCES

(1) Lyu, G.; Wu, S.; Zhang, H. Estimation and Comparison of Bio-Oil Components from Different Pyrolysis Conditions. *Front. Energy Res.* **2015**, *3*, 28.
(2) Lopez-Ruiz, J. A.; Cooper, A. R.; Li, G.; Albrecht, K. O. Enhanced Hydrothermal Stability and Catalytic Activity of LaxZryOz Mixed Oxides for the Ketonization of Acetic Acid in the Aqueous Condensed Phase. *ACS Catal.* **2017**, *7*, 6400−6412.
(3) Alonso, D. M.; Bond, J. Q.; Dumesic, J. A. Catalytic conversion of biomass to biofuels. *Green Chem.* **2010**, *12*, 1493−1513.
(4) Boekaerts, B.; Sels, B. F. Catalytic advancements in carboxylic acid ketonization and its perspectives on biomass valorisation. *Appl. Catal., B* **2021**, *283*, 119607.
(5) Aleem, S. A.; Asikin-Mijan, N.; Hussain, A. S.; Voon, C. H.; Dolfi, A.; Sivasangar, S.; Taufiq-Yap, Y. H. Catalytic ketonization of palmitic acid over a series of transition metal oxides supported on zirconia oxide-based catalysts. *RSC Adv.* **2021**, *11*, 31972−31982.
(6) Boekaerts, B.; Lorenz, W.; Van Aelst, J.; Sels, B. F. Kinetics of fatty acid ketonization in liquid phase with anatase and rutile TiO2 catalysts. *Appl. Catal., B* **2022**, *305*, 121052.
(7) Mansir, N.; Mohd Sidek, H.; Teo, S. H.; Mijan, N.-A.; Ghassan Alsultan, A.; Ng, C. H.; Shamsuddin, M. R.; Taufiq-Yap, Y. H. Catalytically active metal oxides studies for the conversion technology of carboxylic acids and bioresource based fatty acids to ketones: A review. *Bioresour. Technol. Rep.* **2022**, *17*, 100988.
(8) Gliński, M.; Kijeński, J.; Jakubowski, A. Ketones from monocarboxylic acids: Catalytic ketonization over oxide systems. *Appl. Catal., A* **1995**, *128*, 209−217.
(9) Pham, T. N.; Sooknoi, T.; Crossley, S. P.; Resasco, D. E. Ketonization of Carboxylic Acids: Mechanisms, Catalysts, and Implications for Biomass Conversion. *ACS Catal.* **2013**, *3*, 2456−2473.
(10) Pham, T. N.; Shi, D.; Resasco, D. E. Kinetics and Mechanism of Ketonization of Acetic Acid on Ru/TiO_2 Catalyst. *Top. Catal.* **2014**, *57*, 706−714.
(11) Pham, T. N.; Shi, D.; Resasco, D. E. Reaction kinetics and mechanism of ketonization of aliphatic carboxylic acids with different carbon chain lengths over Ru/TiO2 catalyst. *J. Catal.* **2014**, *314*, 149−158.
(12) Wang, S.; Iglesia, E. Experimental and theoretical assessment of the mechanism and site requirements for ketonization of carboxylic acids on oxides. *J. Catal.* **2017**, *345*, 183−206.
(13) Wang, S.; Iglesia, E. Experimental and Theoretical Evidence for the Reactivity of Bound Intermediates in Ketonization of Carboxylic Acids and Consequences of Acid-Base Properties of Oxide Catalysts. *J. Phys. Chem. C* **2017**, *121*, 18030−18046.
(14) Pulido, A.; Oliver-Tomas, B.; Renz, M.; Boronat, M.; Corma, A. Ketonic decarboxylation reaction mechanism: a combined experimental and DFT study. *ChemSusChem* **2013**, *6*, 141−151.
(15) Nagashima, O.; Sato, S.; Takahashi, R.; Sodesawa, T. Ketonization of carboxylic acids over CeO2-based composite oxides. *J. Mol. Catal. A: Chem.* **2005**, *227*, 231−239.
(16) Pham, T. N.; Shi, D.; Sooknoi, T.; Resasco, D. E. Aqueous-phase ketonization of acetic acid over Ru/TiO2/carbon catalysts. *J. Catal.* **2012**, *295*, 169−178.
(17) Ignatchenko, A. V.; Kozliak, E. I. Distinguishing Enolic and Carbonyl Components in the Mechanism of Carboxylic Acid Ketonization on Monoclinic Zirconia. *ACS Catal.* **2012**, *2*, 1555−1562.
(18) Tosoni, S.; Pacchioni, G. Acetic acid ketonization on tetragonal zirconia: Role of surface reduction. *J. Catal.* **2016**, *344*, 465−473.
(19) Bayahia, H.; Kozhevnikova, E. F.; Kozhevnikov, I. V. Ketonisation of carboxylic acids over Zn-Cr oxide in the gas phase. *Appl. Catal., B* **2015**, *165*, 253−259.
(20) Calaza, F. C.; Chen, T.-L.; Mullins, D. R.; Xu, Y.; Overbury, S. H. Reactivity and reaction intermediates for acetic acid adsorbed on CeO2(1 1 1). *Catal. Today* **2015**, *253*, 65−76.
(21) Fufachev, E. V.; Weckhuysen, B. M.; Bruijnincx, P. C. A. Crystal Phase Effects on the Gas-Phase Ketonization of Small Carboxylic Acids over TiO 2 Catalysts. *ChemSusChem* **2021**, *14*, 2710−2720.
(22) Hadjiivanov, K. I.; Klissurski, D. G. Surface chemistry of titania (anatase) and titania-supported catalysts. *Chem. Soc. Rev.* **1996**, *25*, 61−69.
(23) Primet, M.; Pichat, P.; Mathieu, M. V. Infrared study of the surface of titanium dioxides. I. Hydroxyl groups. *J. Phys. Chem.* **1971**, *75*, 1216−1220.
(24) Tamura, H.; Mita, K.; Tanaka, A.; Ito, M. Mechanism of Hydroxylation of Metal Oxide Surfaces. *J. Colloid Interface Sci.* **2001**, *243*, 202−207.
(25) Tamura, H.; Tanaka, A.; Mita, K.-y.; Furuichi, R. Surface Hydroxyl Site Densities on Metal Oxides as a Measure for the Ion-Exchange Capacity. *J. Colloid Interface Sci.* **1999**, *209*, 225−231.
(26) McCafferty, E.; Wightman, J. P. Determination of the concentration of surface hydroxyl groups on metal oxide films by a quantitative XPS method. *Surf. Interface Anal.* **1998**, *26*, 549−564.
(27) Lu, F.; Jiang, B.; Wang, J.; Huang, Z.; Liao, Z.; Yang, Y.; Zheng, J. Promotional effect of Ti doping on the ketonization of acetic acid over a CeO2 catalyst. *RSC Adv.* **2017**, *7*, 22017−22026.
(28) Mino, L.; Spoto, G.; Bordiga, S.; Zecchina, A. Particles Morphology and Surface Properties As Investigated by HRTEM, FTIR, and Periodic DFT Calculations: From Pyrogenic TiO2 (P25) to Nanoanatase. *J. Phys. Chem. C* **2012**, *116*, 17008−17018.
(29) Ohno, T.; Sarukawa, K.; Tokieda, K.; Matsumura, M. Morphology of a TiO2 Photocatalyst (Degussa, P-25) Consisting of Anatase and Rutile Crystalline Phases. *J. Catal.* **2001**, *203*, 82−86.
(30) Jaegers, N. R.; Mueller, K. T.; Wang, Y.; Hu, J. Z. Variable Temperature and Pressure Operando MAS NMR for Catalysis Science and Related Materials. *Acc. Chem. Res.* **2020**, *53*, 611−619.
(31) Jaegers, N. R.; Hu, M. Y.; Hoyt, D. W.; Wang, Y.; Hu, J. Z.Development and Application of In Situ High-Temperature, High-Pressure Magic Angle Spinning NMR. In *Modern Magnetic Resonance*; Springer, 2017; pp 1−19.
(32) Hu, J. Z.; Hu, M. Y.; Zhao, Z.; Xu, S.; Vjunov, A.; Shi, H.; Camaioni, D. M.; Peden, C. H. F.; Lercher, J. A. Sealed rotors for in situ high temperature high pressure MAS NMR. *Chem. Commun.* **2015**, *51*, 13458−13461.
(33) Jaegers, N. R.; Hu, W.; Wang, Y.; Hu, J. Z. High-Temperature and High-Pressure In situ Magic Angle Spinning Nuclear Magnetic Resonance Spectroscopy. *J. Vis. Exp.* **2020**, *164*, 61794.

https://doi.org/10.1021/jacs.2c08511
J. Am. Chem. Soc. 2023, 145, 99−109

(34) Grimme, S.; Ehrlich, S.; Goerigk, L. Effect of the damping function in dispersion corrected density functional theory. *J. Comput. Chem.* **2011**, *32*, 1456−1465.
(35) Becke, A. D. Density-functional exchange-energy approximation with correct asymptotic behavior. *Phys. Rev. A* **1988**, *38*, 3098−3100.
(36) Lee, C.; Yang, W.; Parr, R. G. Development of the Colle-Salvetti correlation-energy formula into a functional of the electron density. *Phys. Rev. A* **1988**, *37*, 785−789.
(37) Van Lenthe, E.; Baerends, E. J. Optimized Slater-Type Basis Sets for the Elements 1-118. *J. Comput. Chem.* **2003**, *24*, 1142−1156.
(38) Jaegers, N. R.; Lai, J.-K.; He, Y.; Walter, E.; Dixon, D. A.; Vasiliu, M.; Chen, Y.; Wang, C.; Hu, M. Y.; Mueller, K. T.; Wachs, I. E.; Wang, Y.; Hu, J. Z. Mechanism by which Tungsten Oxide Promotes the Activity of Supported V 2 O 5 /TiO 2 Catalysts for NO X Abatement: Structural Effects Revealed by 51 V MAS NMR Spectroscopy. *Angew. Chem.* **2019**, *131*, 12739−12746.
(39) Qu, Q.; Geng, H.; Peng, R.; Cui, Q.; Gu, X.; Li, F.; Wang, M. Chemically Binding Carboxylic Acids onto TiO2 Nanoparticles with Adjustable Coverage by Solvothermal Strategy. *Langmuir* **2010**, *26*, 9539−9546.
(40) Zhang, Q.-L.; Du, L.-C.; Weng, Y.-X.; Wang, L.; Chen, H.-Y.; Li, J.-Q. Particle-Size-Dependent Distribution of Carboxylate Adsorption Sites on TiO_2 Nanoparticle Surfaces: Insights into the Surface Modification of Nanostructured TiO_2 Electrodes. *J. Phys. Chem. B* **2004**, *108*, 15077−15083.
(41) Weng, Y.-X.; Li, L.; Liu, Y.; Wang, L.; Yang, G.-Z. Surface-Binding Forms of Carboxylic Groups on Nanoparticulate TiO2 Surface Studied by the Interface-Sensitive Transient Triplet-State Molecular Probe. *J. Phys. Chem. B* **2003**, *107*, 4356−4363.
(42) Dobson, K. D.; McQuillan, A. J. In situ infrared spectroscopic analysis of the adsorption of aliphatic carboxylic acids to TiO_2, ZrO_2, Al_2O_3, and Ta_2O_5 from aqueous solutions. *Spectrochim. Acta, Part A* **1999**, *55*, 1395−1405.
(43) Dobson, K. D.; McQuillan, A. J. In situ infrared spectroscopic analysis of the adsorption of aromatic carboxylic acids to TiO2, ZrO2, Al2O3, and Ta2O5 from aqueous solutions. *Spectrochim. Acta, Part A* **2000**, *56*, 557−565.
(44) Capecchi, G.; Faga, M. G.; Martra, G.; Coluccia, S.; Iozzi, M. F.; Cossi, M. Adsorption of CH_3COOH on TiO_2: IR and theoretical investigations. *Res. Chem. Intermed.* **2007**, *33*, 269−284.
(45) Liao, L.-F.; Lien, C.-F.; Lin, J.-L. FTIR study of adsorption and photoreactions of acetic acid on TiO2. *Phys. Chem. Chem. Phys.* **2001**, *3*, 3831−3837.
(46) Zaki, M. I.; Hasan, M. A.; Pasupulety, L. Surface Reactions of Acetone on Al2O3, TiO2, ZrO2, and CeO2: IR Spectroscopic Assessment of Impacts of the Surface Acid−Base Properties. *Langmuir* **2001**, *17*, 768−774.
(47) Almeida, A. R.; Calatayud, M.; Tielens, F.; Moulijn, J. A.; Mul, G. Combined ATR-FTIR and DFT Study of Cyclohexanone Adsorption on Hydrated TiO2 Anatase Surfaces. *J. Phys. Chem. C* **2011**, *115*, 14164−14172.
(48) Mastikhin, V. M. Characterization of surface active sites of catalysts with high-resolution solid-state NMR. *Colloids Surf., A* **1993**, *78*, 143−166.
(49) Birnie, D. P., III; Bendzko, N. J. 1H and 13C NMR observation of the reaction of acetic acid with titanium isopropoxide. *Mater. Chem. Phys.* **1999**, *59*, 26−35.
(50) Jaegers, N. R.; Wang, Y.; Hu, J. Z. Thermal perturbation of NMR properties in small polar and non-polar molecules. *Sci. Rep.* **2020**, *10*, 6097.
(51) Nosaka, A. Y.; Fujiwara, T.; Yagi, H.; Akutsu, H.; Nosaka, Y. Characteristics of Water Adsorbed on TiO2 Photocatalytic Systems with Increasing Temperature as Studied by Solid-State 1H NMR Spectroscopy. *J. Phys. Chem. B* **2004**, *108*, 9121−9125.
(52) Ye, B. H.; Li, X. Y.; Williams, I. D.; Chen, X. M. Synthesis and Structural Characterization of Di- and Tetranuclear Zinc Complexes with Phenolate and Carboxylate Bridges. Correlations between 13C NMR Chemical Shifts and Carboxylate Binding Modes. *Inorg. Chem.* **2002**, *41*, 6426−6431.
(53) Rorrer, J. E.; Toste, F. D.; Bell, A. T. Mechanism and Kinetics of Isobutene Formation from Ethanol and Acetone over $Zn_xZr_yO_z$. *ACS Catal.* **2019**, *9*, 10588−10604.
(54) Li, H.; Hurlock, M. J.; Sudduth, B.; Li, J.; Sun, J.; Zhang, Q.; Wang, Y. Acetone to isobutene conversion on ZnxTiyOz: Effects of TiO2 facet. *J. Catal.* **2022**, *410*, 236−245.
(55) Huang, R.; Chang, J.; Choi, H.; Vohs, J. M.; Gorte, R. J. Furfural Upgrading by Aldol Condensation with Ketones over Solid-Base Catalysts. *Catal. Lett.* **2022**, *152*, 3833−3842.
(56) Ghosh, T. B.; Dhabal, S.; Datta, A. K. On crystallite size dependence of phase stability of nanocrystalline TiO2. *J. Appl. Phys.* **2003**, *94*, 4577−4582.
(57) Hanaor, D.; Sorrell, C. C. Review of the anatase to rutile phase transformation. *J. Mater. Sci.* **2011**, *46*, 855−874.

https://doi.org/10.1021/jacs.2c08511
J. Am. Chem. Soc. 2023, 145, 99−109